# Supplementary information

## Comparing the Poincaré oscillator with the Hopf oscillator

The results presented in Figures 2 and 3 in the paper show generic features of an oscillator under entrainment. Here, we compare these results with the behaviour of the standard Hopf oscillator. This oscillator is described by the following equations:

$$\frac{dr}{dt} = \lambda r(A_0 - r^2)$$
$$\frac{d\phi}{dt} = \frac{2\pi}{\tau}.$$

Here, $\lambda$ is the amplitude relaxation rate, $A_0$ is the amplitude, and $\tau$ is the oscillator period. In Figure S1 we numerically calculated the entrainment region (known as the 1:1 Arnold tongue) for the Hopf oscillator as a function of the zeitgeber strength and zeitgeber period. As zeitgeber we used square pulses, i.e. an entrainment signal of period $T$ is sculpted as a $T/2$ h on : $T/2$ h off square wave. The magnitude of the "on" state is the zeitgeber strength. Consistent with the results presented in Figure 2 of the paper, here the weak oscillator, i.e. the one with smaller $\lambda$, has a larger entrainment region whereas the rigid oscillator has a smaller entrainment region.

## Comparing the generic oscillators with a biophysical model of coupled circadian oscillators

In order to further justify the use of the generic Poincaré oscillator model in the simulations (and in the analytical treatment below), we wished to assert that its behavior is consistent with that of a biophysically motivated circadian clock model. To this end, we followed Bernard *et al.* (2007), and studied two coupled mammalian circadian oscillators, each one as originally modeled by Becker-Weimann *et al.* (2004). To this original model, Bernard *et al.* (2007) introduced cell-to-cell coupling via a neurotransmitter, and obtained this system of coupled ordinary differential equations:

$$
\begin{aligned}
\frac{dy_{1,j}}{dt} &= \frac{v_{1\mathrm{b}}(y_{7,j} + x_{2,j}^h/k_{x1\mathrm{i}})}{k_{1\mathrm{b}}\left(1 + (y_{3,j}/k_{1\mathrm{i}})^p\right) + y_{7,j} + x_{2,j}^h/k_{x1\mathrm{i}}} - k_{1\mathrm{d}}y_{1,j} + F \\
\frac{dy_{2,j}}{dt} &= k_{2\mathrm{b}}y_{1,j}^q - k_{2\mathrm{d}}y_{2,j} - k_{2\mathrm{t}}y_{2,j} + k_{3\mathrm{t}}y_{3,j} \\
\frac{dy_{3,j}}{dt} &= k_{2\mathrm{t}}y_{2,j} - k_{3\mathrm{t}}y_{3,j} - k_{3\mathrm{d}}y_{3,j} \\
\frac{dy_{4,j}}{dt} &= \frac{v_{4\mathrm{b}}y_{3,j}^r/k_{4\mathrm{b}}^r}{1 + y_{3,j}^r/k_{4\mathrm{b}}^r} - k_{4\mathrm{d}}y_{4,j} \\
\frac{dy_{5,j}}{dt} &= k_{5\mathrm{b}}y_{4,j} - k_{5\mathrm{d}}y_{5,j} - k_{5\mathrm{t}}y_{5,j} + k_{6\mathrm{t}}y_{6j} \\
\frac{dy_{6,j}}{dt} &= k_{5\mathrm{t}}y_{5,j} - k_{6\mathrm{d}}y_{6,j} - k_{6\mathrm{t}}y_{6,j} + k_{7\mathrm{a}}y_{7,j} - k_{6\mathrm{a}}y_{6,j} \\
\frac{dy_{7,j}}{dt} &= k_{6\mathrm{a}}y_{6,j} - k_{7\mathrm{a}}y_{7,j} - k_{7\mathrm{d}}y_{7,j} \\
\frac{dv_j}{dt} &= k_8y_{2,j} - k_{8\mathrm{d}}v_j \\
\frac{dx_{1,j}}{dt} &= k_{x1}Q\left(x_{1\mathrm{T}} - x_{1,j}\right) - k_{\mathrm{d}x1}x_{1,j} \\
\frac{dx_{2,j}}{dt} &= k_{x2}x_{1,j}\left(x_{2\mathrm{T}} - x_{2,j}\right) - k_{\mathrm{d}x2}x_{2,j}.
\end{aligned}
$$

In all, this model accounts for the mRNA of clock proteins, e.g. Per or Cry ($y_1$), the corresponding cytosolic ($y_2$), and nuclear proteins ($y_3$). The nuclear clock proteins inhibit the production of their own messages: this is why find the variable $y_3$ in the denominator of the Hill function that describes the production of $y_1$. This core negative feedback loop is supplemented by interlocked positive loops, here modeled as being formed between clock proteins and the bHLH transcription factor BMAL: the production of BMAL mRNA ($y_4$) is assumed to be stimulated by nuclear clock protein ($y_3$). This stimulation forms a positive feedback loop, since cytosolic BMAL ($y_5$) and free nuclear BMAL ($y_6$) finally lead to the DNA-bound *cis*-activating form ($y_7$), which activates the transcription of clock protein mRNA. The activation of BMAL transcription by clock proteins could occur via clock-protein induced transcriptional repression of inhibitors of BMAL transcription, such as Rev-erb$\alpha$ (Reppert and Weaver, 2002). However, a great number of different positive feedback routes are conceivable (Ueda *et al.*, 2005). The variables $y_1$ to $y_7$ with the interlocked negative and positive feedback loop represent the core mammalian circadian clock. To the original Becker-Weimann model, Bernard *et al.* (2007) added a module that describes cell-to-cell coupling, assumed to be mediated by a neurotransmitter $v$ (Welsh *et al.*, 2010), modeled to follow the dynamics of the cytosolic clock protein $y_2$. As elsewhere in the paper, we considered coupling of two oscillators; $j = 1$ or 2. If diffusion of neuropeptide is fast compared to the circadian time scale, the oscillators experience an averaged

(mean field) concentration $Q$ of the secreted neuropeptides:

$$Q = \frac{K}{2}\left(v_1 + v_2\right),$$

where $K$ is the coupling strength. The mean field $Q$ is modeled to activate an intracellular two-step cascade, schematized as PKA ($x_1$) and CREB ($x_2$) activation, which in turn is assumed to activate transcription of clock protein mRNA ($y_1$).

The parameters of the model were exactly as in the original report (Bernard *et al.*, 2007), namely: $v_{1b} = 9.0$, $k_{1b} = 1.0$, $k_{1i} = 0.56$, $p = 3$, $h = 2$, $k_{x1i} = 1$, $k_{1d} = 0.18$, $k_{2b} = 0.3$, $q = 2$, $k_{2d} = 0.1$, $k_{2t} = 0.36$, $k_{3t} = 0.02$, $k_{3d} = 0.18$, $v_{4b} = 1.0$, $k_{4b} = 2.16$, $r = 3$, $k_{4d} = 1.1$, $k_{5b} = 0.24$, $k_{5d} = 0.09$, $k_{5t} = 0.45$, $k_{6t} = 0.06$, $k_{6d} = 0.18$, $k_{6a} = 0.09$, $k_{7a} = 0.003$, $k_{7d} = 0.13$, $k_8 = 1.0$, $k_{8d} = 4.0$, $k_{x1} = 3.0$, $x_{1T} = 15.0$, $k_{dx1} = 4.0$, $k_{x2} = 0.25$, $x_{2T} = 15.0$, $k_{dx2} = 10.0$. The unit of these parameters is $\mathrm{h}^{-1}$, except $k_{x1i}$ ($\mathrm{nM}^{(h-1)}$); $k_{2b}$ ($\mathrm{h}^{-1}\mathrm{nM}^{-(q-1)}$); $k_{1b}$, $k_{1i}$, and $k_{4b}$ (nM); $k_{x1}$ and $k_{x2}$ ($\mathrm{h}^{-1}\mathrm{nM}^{-1}$); $v_{1b}$, $v_{4b}$, and $F$ ($\mathrm{nM\,h}^{-1}$); and $x_T$ (nM). The external entrainment signal $F$ is in this model assumed to act on the transcription of clock proteins. We studied the unforced system ($F = 0$), as well as the forced system with $F$ being a square waveform with period $T$, during which it alternates between 0 and 0.03 with equal durations. Forcing period $T$ and coupling strength $K$ were varied, in order to analyze this model's behaviour in relation to that of the Poincaré model.

We set out to qualitatively replicate Figure 5 of the paper with this model. First, we studied the unforced coupled system. This system is damped for low coupling strengths, producing self-sustained oscillations only for $K > 0.4941\ \mathrm{h}^{-1}$. This is in line with experimental findings that SCN neurons lose their coherent self-sustained rhythm when coupling is severed (Liu *et al.*, 2007; Webb *et al.*, 2009). Figure S2A shows how the relative oscillation amplitude of $y_1$ (amplitude divided by mean) of the unforced system increases as the coupling strength further increases, as is the case for the Poincaré oscillator (Figure 5A in the paper). We proceeded to calculate the amplitude relaxation rate of the oscillator (i.e. the Floquet exponent representing the slowest time scale), as a function of coupling strength (using Cl_MatCont (Dhooge *et al.*, 2008), see the Materials and methods section of the paper). The result is shown in figure S2B, and demonstrates a strong, dependence of the relaxation rate on the coupling strength, much like for the Poincaré oscillator (Figure 5B of the paper). Finally, we studied the lower limit of entrainment as a function of the coupling strength, and found that the entrainment range decreases with increasing coupling strength, again in qualitative agreement with the results obtained for the Poincaré oscillator (Figure 5C of the paper). The lower limit of entrainment (a torus bifurcation in this case) takes a dramatic turn and for low coupling strengths, the system is close to being damped and can entrain to almost any forcing period $T$. Such behaviour has been studied earlier, e.g. in the context of forced coupled Duffing oscillators (Kozlowski *et al.*, 1995). As for the calculations in Figure 5C, we normalized the lower limit of entrainment to the period of the unforced system at corresponding coupling strengths, then multiplying with 24 hours, since coupling somewhat increases the period of the unforced system itself. This period change otherwise slightly exaggerates the

effect of the coupling on the lower limit of entrainment. See the Materials and methods section of the paper for details.

## Entrainment: analytical expressions

In this section we outline an analytical approach that captures many of the previous results and sets a theoretical framework for entrainment studies. Our goal in this section is to show that the presented results represent generic oscillator properties. We consider a general oscillator model with minimal assumptions and study its entrainment properties. The mathematical approach presented here has successfully been used to study other oscillator models such as the well-known van der Pol oscillator. For a comprehensive introduction to the study of forced oscillators, see Balanov *et al.* (2009), where much of the theory below is outlined. For clarity the oscillator is described in radial coordinates, with radial evolution $\frac{dr}{dt} = f(r)$ and phase evolution $\frac{d\phi}{dt} = \omega_0$, where $f(r)$ describes the radial dynamics and $\omega_0$ is the oscillator frequency (in all numerical calculations taken to be $2\pi/24$ $\mathrm{h}^{-1}$). The entrainment signal is applied in the x-coordinate direction and is a sinusoidal function $B\sin(\Omega t)$ with the zeitgeber strength $B$, the zeitgeber frequency $\Omega$ and time $t$. Note that $\omega_0 = \frac{2\pi}{\tau}$ and $\Omega = \frac{2\pi}{T}$, where $\tau$ is the oscillator intrinsic period and $T$ the zeitgeber period. The oscillator equations under entrainment take the form:

$$\begin{aligned}\frac{dr}{dt} &= f(r) + B\sin(\Omega t)\cos(\phi)\\ \frac{d\phi}{dt} &= \omega_0 - \frac{B\sin(\Omega t)}{r}\sin(\phi).\end{aligned}$$

Here, $r$ and $\phi$ describe the radius and the phase under periodic forcing. When an oscillator is entrained, it reaches a stable phase relation with the zeitgeber and thus their phase difference becomes constant. Therefore, in order to study entrainment it is convenient to rewrite these equations as phase difference equations. Thus we define $\psi = \phi - \Omega t$ as the phase difference between the entrainment signal and the forced oscillators. We have

$$\begin{aligned}\frac{dr}{dt} &= f(r) + B\sin(\Omega t)\cos(\psi + \Omega t)\\ \frac{d\psi}{dt} &= \Delta - \frac{B}{r}\sin(\Omega t)\sin(\psi + \Omega t),\end{aligned}$$

where $\Delta = \omega_0 - \Omega$ is defined as detuning. Assuming that the phase difference $\psi(t)$ and radial dynamics $r(t)$ have a much slower timescale than the entrainment signal, we can use the averaging method developed by Krylov and Bogoliubov as used by Balanov *et al.* (2009). After averaging the phase difference equations lead to:

$$\frac{d\bar{r}}{dt} = f(\bar{r}) + \frac{B}{2}\cos(\bar{\psi}) \tag{S1}$$

$$\frac{d\bar{\psi}}{dt} = \Delta - \frac{B}{2\bar{r}}\sin(\bar{\psi}). \tag{S2}$$

Here, $\bar{r}$ and $\bar{\psi}$ describe the forced averaged radial and phase dynamics, respectively. For simplicity, in the following we keep the non-averaged notation $r$ and $\psi$. In the entrained state both the entrained amplitude and phase are constant, i.e. $\frac{d\psi}{dt} = 0$ and $\frac{dr}{dt} = 0$. Note that $r(t)$ depends on the specific radial dynamics described by $f(r)$. Nevertheless, without specifying $f(r)$ but assuming that $r(t) \simeq A_0$ near the borders of the entrainment region (see Figure 2B of the paper) we obtain an expression for the lower limit of entrainment:

$$T_{\text{Low}} = \frac{\tau}{1 + \frac{B\tau}{4\pi A_0}}. \tag{S3}$$

With this equation we can plot the predicted lower limit of entrainment $T_{\text{Low}}$ as a function of the ratio between zeitgeber strength and oscillator amplitude and compare it to simulations from different oscillator models. In Figure S3 a good agreement between simulation results from three oscillator models (linear, i.e. with radial dynamics described by $f(r) = \lambda(A_0 - r)$, Poincaré, and Hopf-like oscillator) and the theoretically predicted curve is observed. To obtain an analytical expression that correctly describes the dependence of the lower limit of entrainment on the ratio zeitgeber strength to oscillator amplitude we used an averaging method that averages out the dependence on $\lambda$. Thus, contrary to the results presented in the main text of the paper, Equation S3 does not describe the dependence of the lower limit of entrainment on the radial relaxation rate $\lambda$.

Moreover, the phase of entrainment can be deduced from the averaged phase dynamics, Equation S2. Assuming again that $r(t) \simeq A_0$ near the borders of the entrainment region (see Figure 2B) we find the stable phase of entrainment as the solution of $\Delta = \frac{B}{2A_0}\sin(\psi_{\text{ent}})$ that leads to:

$$\psi_{\text{ent}} = \arcsin\left(\frac{2A_0\Delta}{B}\right).$$

Furthermore, we can specify in Equation S1 a particular oscillator model and calculate the entrained amplitude. As an example, for the linear oscillator with radial dynamics described by $f(r) = \lambda(A_0 - r)$, the entrained amplitude is

$$A_{\text{ent}} = \frac{\lambda^2 A_0}{\lambda^2 + \Delta^2} + \sqrt{\frac{\left(2\lambda^2 A_0\right)^2 - \left(\lambda^2 + \Delta^2\right)\left(4\lambda^2 A_0^2 - B^2\right)}{4\left(\lambda^2 + \Delta^2\right)^2}}.$$

In Figure 2B of the paper, we plotted this analytical expression of the entrained amplitude $A_{\text{ent}}$ for a weak and rigid oscillator together with simulations results and found a good agreement. The entrained amplitude will reach a maximum when the zeitgeber period equals the oscillator period, i.e. $\Delta = 0$ , and a minimum at the limits of entrainment.

Note that the approximation $r \simeq A_0$ is valid at the limits of the entrainment region, for small zeitgeber strength or for large radial relaxation rates (in our simulations, $\lambda \gtrsim 0.03$).

## Supplementary materials and methods

### *In vitro* tissue culture

We cultured SCN and lung tissues from mice as described elsewhere with a few modifications (Abe *et al.*, 2002). Briefly, animals were sacrificed via cervical dislocation and their brains and lungs transferred to chilled Hank's buffered saline solution (HBSS, pH 7.2, Sigma) supplemented with 0.01 M HEPES (Sigma), 100 units/ml penicillin and 0.1 mg/ml streptomycin, and 4 mM $NaHCO_3$ (Invitrogen, Carlsbad, CA). For tissue culture, 300 µm coronal sections of the brain and lung were obtained with a tissue chopper (McIllwain, UK). The brain slice containing the SCN was identified, and the bilateral, medial SCN dissected out using a pair of scalpels. All tissues were cultured individually on a Millicell membrane (Millipore, Bedford, MA, USA) in a petri dish with 1 ml of Dulbecco's Modified Eagle's Medium (Sigma) supplemented with 10 ml B27 supplement (50x, Invitrogen, Carlsbad, USA), 10 mM Hepes (Sigma), 2.2 mg/ml $NaHCO_3$ (Invitrogen, Carlsbad, USA) and 0.1 mM beetle luciferin (BioThema, Handen, Sweden). Petri dishes were covered with glass slides, sealed with grease and placed under temperature adjustable photomultiplier tubes (HC135-11MOD, Hamamatsu, Shizouka, Japan, modified by Technische Werkstätten Charité, Berlin, Germany) at 37 °C, 5% $CO_2$ in the dark. Bioluminescence was recorded in 5 min bins for at least 12 days. SCN slices were incubated in 1 ml DMEM at 37 °C, 5% $CO_2$ for about 3 weeks prior to the start of the bioluminescence recording to allow the slice culture to consolidate, while recording of lung cultures started 1 to 7 days after dissection.

### Entrainment to different strengths of the temperature zeitgeber

In order to investigate entrainment with different zeitgeber strengths, PER2::LUCIFERASE SCN and lung slices were recorded at a constant temperature of 37 °C as described. After the second or third peak of PER2::LUC bioluminescence temperature was decreased to a final level of 36.25 °C to 29 °C (cold phase) depending on the respective zeitgeber strength ($\Delta$T) applied. The cold phase lasted for 10 ($T$ = 20 hours) or 11 hours ($T$ = 22 hours) before temperature increased again to 37 °C for 10 or 11 hours. Temperature entrainment comprised six cycles before a constant 37 °C was assumed. The first cold phase started at the minimum of PER2::LUC bioluminescence as determined by online registration. In order to simulate gradual temperature changes at dusk and dawn, each 10-hour or 11-hour temperature phase was preluded by a 2-hour gradual increase or decrease of the temperature.

### Forskolin stimulation

To investigate phase changes of SCN and lung slices in response to a chemical stimulus, cultures received single injections of forskolin (Sigma), an activator of adenylyl cyclase which increases intracellular cyclic AMP levels. Forskolin has been shown to perturb clock functions in peripheral and central oscillators before

(Obrietan *et al.*, 1999; Yagita and Okamura, 2000; Brown *et al.*, 2008). Injections were performed exactly 6 hours after peak bioluminescence of the respective culture as determined by online registration. 100 $\mu$l of culture medium containing different forskolin concentration were injected through a small hole in the lid of the dish to obtain final concentrations of 0.05 $\mu$M, 0.2 $\mu$M, or 10 $\mu$M forskolin, respectively, in the dishes. During the procedure, the dishes were not removed from the incubator and the online registration was not disturbed. Each culture received only a single forskolin stimulus. Cultures were kept at a constant 37 °C at all times. Phase changes in response to forskolin stimulation were determined by calculating the differences between predicted (extrapolations using the peak period before stimulation) and actually measured peak phases following stimulation. Forskolin injections resulted in either phase delays or advances of the predicted peaks.

**Single cell recordings and data evaluation**

PER2::LUC mice were sacrificed by cervical dislocation, their brains removed, collected in chilled HBSS, and sectioned at 300 µm using a McIllwain tissue chopper. SCN tissue was dissected out as described above and placed on a piece of Millicell membrane located on an intact Millicell membrane insert in 1 ml of DMEM (specifications see above). Slices were incubated at 37 °C/5% $CO_2$ for about 2 days. Subsequently, SCN on Millicell membrane pieces were inverted and cultured in 100 $\mu$l DMEM on the bottom of poly-D-lysine/5% laminine-coated 35 mm IBIDI tissue culture dishes with grid. Again, slices were incubated at 37 °C/5% $CO_2$ and the culture medium exchanged daily. On day 3–5, the culture medium was replaced by 500 $\mu$l DMEM supplemented with 0.18 mg/ml $NaHCO_3$ and 0.1 mM beetle luciferin (BioThema, Handen, Sweden), the petri dish was sealed with grease and placed in a light-tight imaging chamber. Bioluminescence imaging was carried out in complete darkness with a 10x objective and an inverse setup including an intensified digital camera (XR/Mega-10Z, Stanford Photonics, CA, USA). Temperature was kept constant at 37 °C using thin transparent glass heaters (Cell Micro Controls, VA, USA) placed on the lid of the petri dish. Images were stored in 10 min bins over the course of several days. For MDL-treatment, culture medium was exchanged by DMEM supplemented with 0.1 mM beetle luciferin and 10 $\mu$M MDL (Sigma, St. Louis, USA) and imaging was resumed immediately.

10 min exposures were stacked and resulting movies smoothed using a 15 image running average (Piper 1.3. software, Stanford Photonics, USA) or, alternatively, raw movies were subjected twice to a Kalman filter (ImageJ software, NIH, USA). Raw time-series data were visually inspected and only cells that displayed (i) at least $x - 2$ peaks with a period roughly between 18–30 hours ($x$ = number of days recorded) and (ii) not more than one double-peak (2 peaks in 24 hours of recording time) were included in further analysis. Note that due to technical limitations cells tracked before and after MDL-treatment were not identical.

**Numerical Calculations**

The biophysical Becker-Weimann-Bernard model was analyzed using the Matlab toolbox Cl_MatCont (Dhooge *et al.*, 2008). The phase response curve presented in Figure S3A was numerically calculated using the Poincaré oscillator described by Equation 1 of the paper, with $A_0 = 1$ under horizontal square-like perturbations. Both the weak ($\lambda = 0.03\ \mathrm{h}^{-1}$) and the rigid version ($\lambda = 1\ \mathrm{h}^{-1}$) were perturbed at 60 different phases with square pulses of 2 h and amplitude $0.5\ \mathrm{h}^{-1}$ and their phase changes were estimated as described by Granada *et al.* (2009). In Figure S5A, the phase of entrainment was calculated for a weak Poincaré oscillator entrained to sinusoidal cycles (see Materials and methods in the paper) applied in the horizontal coordinate. We use a zeitgeber period of 20 h and an increasing zeitgeber strength from 0 to $0.4\ \mathrm{h}^{-1}$. As phase marker we use the mean value crossing of the entrained oscillator (after transient time) calculated with the Rob Clewley's "getcrossings.m" Matlab function. The phase of entrainment is calculated here as the stable phase difference between the phase of the zeitgeber and the phase of the entrained oscillator, i.e. $\Delta\phi = \phi_{\mathrm{zeitgeber}} - \phi_{\mathrm{oscillator}}$. Thus a phase advance result in an earlier crossing time and a phase delay in a later crossing time. In Figure S8B we calculated the phase of entrainment as a function of the oscillator radial relaxation rate $\lambda$. Here a Poincaré oscillator was entrained to sinusoidal cycles of 20 h and amplitude $0.2\ \mathrm{h}^{-1}$ and the phase of entrainment was calculated as described above.

# References


Abe M, Herzog ED, Yamazaki S, Straume M, Tei H, Sakaki Y, Menaker M, Block GD (2002) Circadian rhythms in isolated brain regions. *J Neurosci* **22**: 350–356

Balanov A, Janson N, Postnov D, Sosnovtseva O (2009) *Synchronization: From Simple to Complex*. Springer-Verlag, New York

Becker-Weimann S, Wolf J, Herzel H, Kramer A (2004) Modeling feedback loops of the mammalian circadian oscillator. *Biophys J* **87**: 3023–3034

Bernard S, Gonze D, Čajavec B, Herzel H, Kramer A (2007) Synchronization-induced rhythmicity of circadian oscillators in the suprachiasmatic nucleus. *PLoS Comput Biol* **3**: e68

Brown SA, Kunz D, Dumas A, Westermark PO, Vanselow K, Tilmann-Wahnschaffe A, Herzel H, Kramer A (2008) Molecular insights into human daily behavior. *Proc Natl Acad Sci USA* **105**: 1602–1607

Dhooge A, Govaerts W, Kuznetsov YA, Meijer HGE, Sautois B (2008) New features of the software matcont for bifurcation analysis of dynamical systems. *Mathematical and Computer Modelling of Dynamical Systems: Methods, Tools and Applications in Engineering and Related Sciences* **14**: 147–175

Granada A, Hennig RM, Ronacher B, Kramer A, Herzel H (2009) Phase response curves elucidating the dynamics of coupled oscillators. *Methods Enzymol* **454**: 1–27

Kozlowski J, Parlitz U, Lauterborn W (1995) Bifurcation analysis of two coupled periodically driven Duffing oscillators. *Phys Rev E* **51**: 1861–1867

Liu AC, Welsh DK, Ko CH, Tran HG, Zhang EE, Priest AA, Buhr ED, Singer O, Meeker K, Verma IM, Doyle FJ 3rd, Takahashi JS, Kay SA (2007) Intercellular coupling confers robustness against mutations in the SCN circadian clock network. *Cell* **129**: 605–616

Obrietan K, Impey S, Smith D, Athos J, Storm DR (1999) Circadian regulation of cAMP response element-mediated gene expression in the suprachiasmatic nuclei. *J Biol Chem* **274**: 17748–17756

Reppert SM, Weaver DR (2002) Coordination of circadian timing in mammals. *Nature* **418**: 935–941

Ueda HR, Hayashi S, Chen W, Sano M, Machida M, Shigeyoshi Y, Iino M, Hashimoto S (2005) System-level identification of transcriptional circuits underlying mammalian circadian clocks. *Nat Genet* **37**: 187–192

Webb AB, Angelo N, Huettner JE, Herzog ED (2009) Intrinsic, nondeterministic circadian rhythm generation in identified mammalian neurons. *Proc Natl Acad Sci U S A* **106**: 16493–16498

Welsh DK, Takahashi JS, Kay SA (2010) Suprachiasmatic nucleus: cell autonomy and network properties. *Annu Rev Physiol* **72**: 551–577

Yagita K, Okamura H (2000) Forskolin induces circadian gene expression of rPer1, rPer2 and dbp in mammalian rat-1 fibroblasts. *FEBS Lett* **465**: 79–82

**Figures S1-S8**

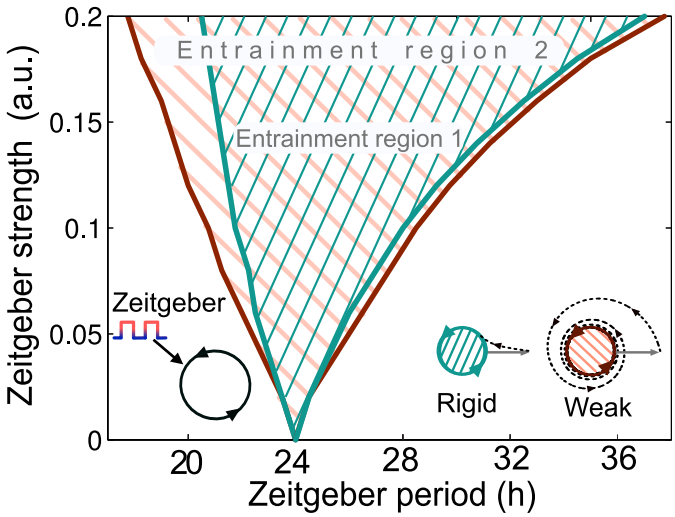


Figure S1: Numerically calculated entrainment zone for the Hopf oscillator. The entrainment region is plotted as a function of the zeitgeber strength and period, also known as the 1:1 Arnold tongue. Weaker oscillators (smaller $\lambda$) exhibit a broader entrainment region. Computational details are given in the Materials and methods section of the paper.

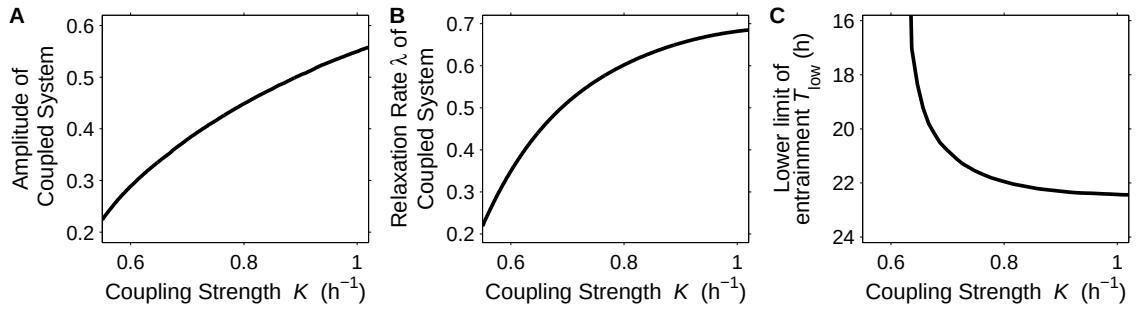


Figure S2: Replication of Figure 5 of the paper, for the biophysically motivated Becker-Weimann-Bernard model (Bernard *et al.*, 2007). Two coupled oscillators were modeled, and the following dependences on the coupling strength $K$ were studied: (**A**) the unforced relative amplitude of the variable $y_1$; (**B**) the unforced relaxation rate; and (**C**) the lower limit of entrainment of the forced system.

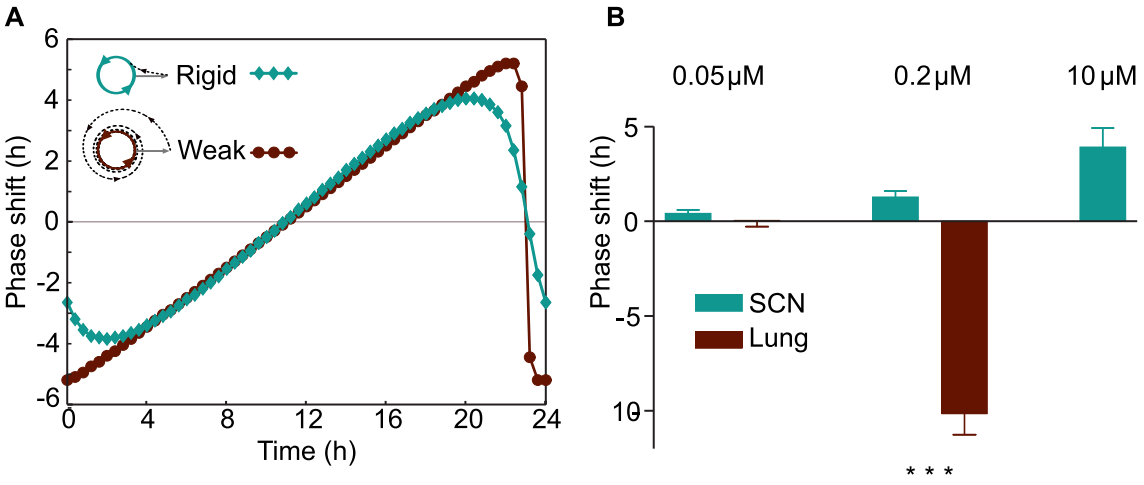


Figure S3: A chemical zeitgeber elicits differential responses in weak and strong oscillators. (**A**) The amplitude of the phase response curve depends on the oscillator radial relaxation rate. A phase response curve (PRC) describes how perturbations shift the phase of the oscillator. Weak oscillators (dots) suffer stronger phase shifts to perturbations than do rigid oscillators (diamonds). The peak-to-trough amplitude of the weak oscillator PRC (from the maximum phase delay to the maximum phase advance) is about 10 h whereas the PRC peak-to-trough amplitude of the rigid oscillator is 8 h. Note that this difference in the PRC peak-to-trough amplitude is consistent with the entrainment range difference shown in Figure 2A. Both PRCs were numerically calculated using the Poincaré oscillator described by Equation 1 of the paper, with radius $A_0 = 1$. The phase changes were estimated as described by Granada *et al.* (2009). When applying perturbations in order to calculate the PRC, we used an horizontal square pulse of amplitude 0.5 $h^{-1}$ and 2 hours length. Computational details are given in Supplementary Material and methods. (**B**) Lung and SCN react differently in response to forskolin (an activator of cAMP-dependent signaling pathways) as a zeitgeber. Injections of either 0.05 $\mu$M forskolin to the culture media of SCN and lung slices resulted in no phase shifts of circadian PER2::LUCIFERASE oscillations in both lung and SCN, while 0.2 $\mu$M resulted in significantly large phase delays in lung slices and small phase advances in SCN slices (Kruskal-Wallis-statistics, $p < 0.001$). With reference to (A) these data confirm experimentally that weak oscillators (lung slices) respond with larger phase shifts than rigid oscillators (SCN slices). SCN slices are able to respond substantially to forskolin stimulation as shown by the phase advances in response to the application of 10 $\mu$M forskolin. In fact, SCN phase responses to forskolin stimulation appear to be dose-dependent.

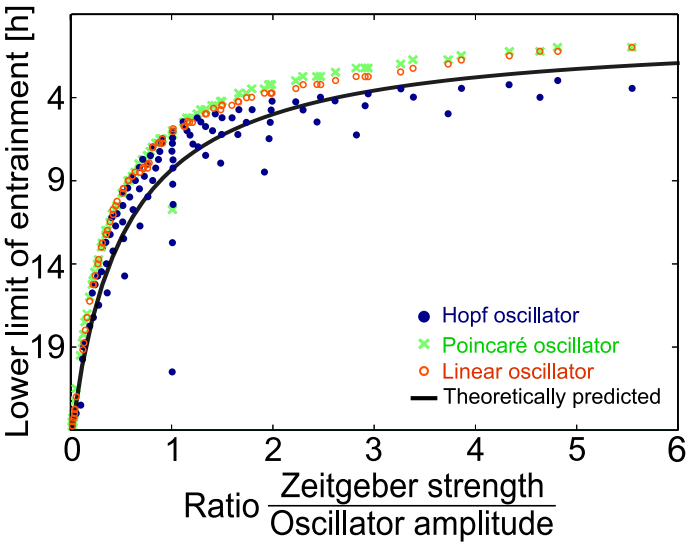


Figure S4: Lower limit of entrainment ($T_{\mathrm{Low}}$) as a function of the zeitgeber to oscillator amplitude ratio. The theoretically predicted curve (black solid line) is plotted together with numerically calculated (dots) lower limit of entrainment from a linear, Hopf and Poincaré oscillator with $\lambda = 0.01$ h$^{-1}$. Further computational details can be found in the Materials and methods section of the paper.

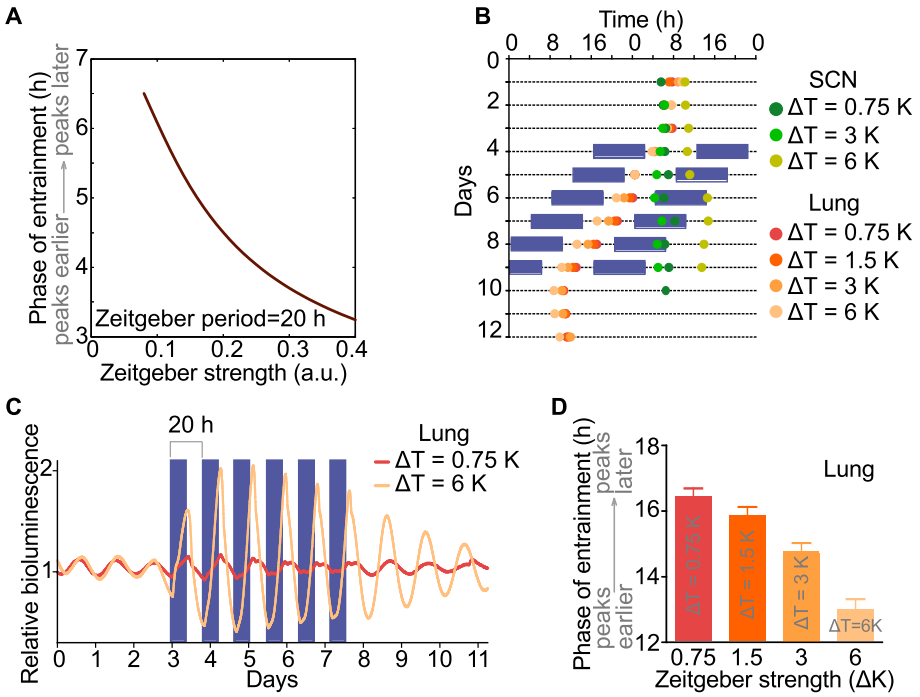


Figure S5: Entrainment properties are dependent on zeitgeber strength. (**A**) Numerically calculated phase of entrainment for a Poincaré oscillator (see Equation 1 of the paper) as a function of the zeitgeber strength. Stronger zeitgebers advance the phase of entrainment resulting in an earlier peaking time of the oscillation. For this simulation we study a weak oscillator ($\lambda = 0.03$ $h^{-1}$) of radius $A_0 = 1$ and fixed the zeitgeber period to 20 h. Computational details are given in Supplementary Material and methods. (**B**) Entrainment of lung tissue to $T$ = 20 hour zeitgeber cycles. Peak times of PER2::LUCIFERASE bioluminescence derived from four individual lung slices and three individual SCN slices. Between days 4 and 9, in vitro cultures were subjected to 20-hour temperature cycles with 10 hours cold phases (blue boxes) of 36.25 °C (ΔT = 0.75 K), 35.5 °C (ΔT = 1.5 K, lung only), 34 °C (ΔT = 3 K), or 31 °C (ΔT = 3 K), respectively, alternating with 10-h warm phases of 37 °C. Following day 9, cultures were kept at a constant 37 °C. All four lung tissues fully entrained to the temperature cycles, while none of the SCN tissues did. (**C**) Time-series of relative PER2::LUCIFERASE bioluminescence derived from two lung slices shown in (B). Cultures were subjected to 20-h temperature cycles (blue box = cold phase) with ΔT= 0.75 K (red) and ΔT = 6 K (orange). Note the different phase angles of entrainment to the zeitgeber: the tissue subjected to the stronger zeitgeber (ΔT = 6 K) peaks earlier than the tissue exposed to the weaker zeitgeber (ΔT = 0.75 K). In addition, the stronger zeitgeber elicits a pronounced amplitude expansion in PER2::LUCIFERASE during entrainment. (**D**) Phase angles of entrainment (hours after onset of the cold phase) of the lung slices shown in (B). Means ± s.e.m. of the last four days of entrainment show a zeitgeber dose-dependent effect: the stronger the zeitgeber, the earlier the peak phase.

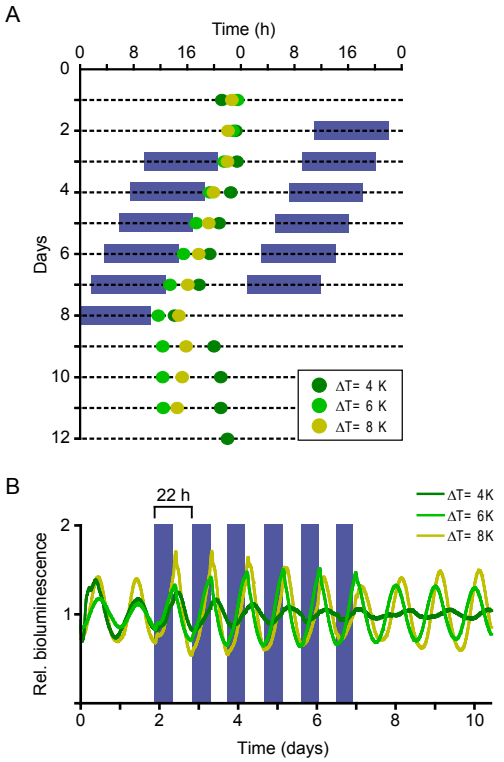


Figure S6: The SCN entrains to a $T$ = 22 hour zeitgeber cycle. (**A**) Peak times of PER2::LUCIFERASE bioluminescence derived from three individual SCN slices. Between days 3 and 8, in vitro cultures were subjected to 22-hour temperature cycles with 11 hours cold phases (blue boxes) of 33 °C ($\Delta$T = 4 K), 31 °C ($\Delta$T = 6 K), and 29 °C ($\Delta$T = 8 K), respectively, alternating with 11 hours warm phases of 37 °C. Following day 8, cultures were kept at a constant 37 °C. The SCN slices subjected to the two stronger zeitgebers ($\Delta$T = 6 K, light green, and $\Delta$T = 8 K, olive) entrained to the temperature cycles, while the SCN exposed to the weaker zeitgeber ($\Delta$T = 4 K, green) assumed a stable phase relationship with the temperature cycles, which, however, did not transfer when the cultures were released into constant 37 °C. Hence, the SCN with $\Delta$T = 4 K was "masked" by the temperature cycle, but did not entrain to the $T$ = 22 hour temperature cycle. (**B**) Time-series of relative PER2::LUCIFERASE bioluminescence derived from all three SCN slices shown in (A). Cultures were subjected to 22 hour temperature cycles (blue box = cold phase) with $\Delta$T = 4 K (green), $\Delta$T = 6 K (light green), and $\Delta$T = 8 K (olive). Note the different phase angles of entrainment to the zeitgeber: the tissue subjected to the stronger zeitgeber ($\Delta$T = 8 K) peaks later than the tissue exposed to the weaker zeitgeber ($\Delta$T = 6 K). This is in contrast to the situation in lung tissue (see Figure S5). As noted in (A), peak bioluminescence of the SCN slice with the lowest zeitgeber strength ($\Delta$T = 4 K) was masked, but not entrained by the temperature cycles. Compared to lung slices, entrainment did not elicit a pronounced increase in PER2::LUCIFERASE amplitude, but somehow reduced the damping (as it can be seen in the non-entrained $\Delta$T = 4 K case) substantially.

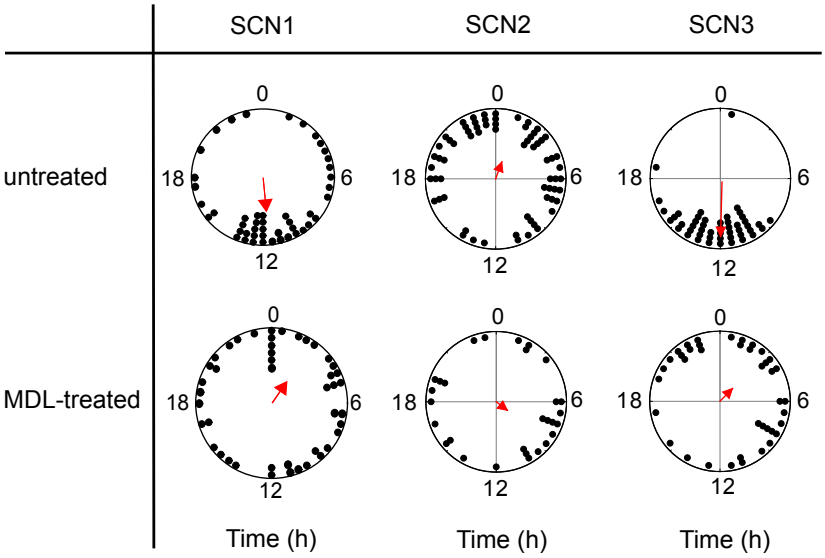


Figure S7: Pharmacological decoupling of SCN cells leads to de-phasing of single cell oscillations. Single cell analyses of three different SCN slices were performed independently, one of which is also presented in Figure 6C. Polar plots show the peak times of PER2-driven bioluminescence of individual SCN cells during the third day of slice recording. Each dot represents the phasing of a single cell. Single cell phases in the untreated SCN slice (upper panel) clustered significantly (Rayleigh test: SCN1: $r = 0.46$, $p < 0.001$, $n = 46$; SCN2: $r = 0.26$, $p < 0.05$, $n = 67$; SCN3: $r = 0.8$, $p < 0.0001$, $n = 49$), but were randomly distributed during MDL-treatment (lower panel; Rayleigh test: SCN1: $r = 0.23$, $p > 0.05$, $n = 45$; SCN2: $r = 0.2$, $p = 0.3$, $n = 30$; SCN3: $r = 0.26$, $p = 0.07$, $n = 40$). Arrows in polar plots represent the mean vectors; the direction denotes the mean phase, and length measures the tendency of the data to cluster based upon a Rayleigh test where $r$ values range from 0 (randomly phased) to 1 (all cells peak at the same time).

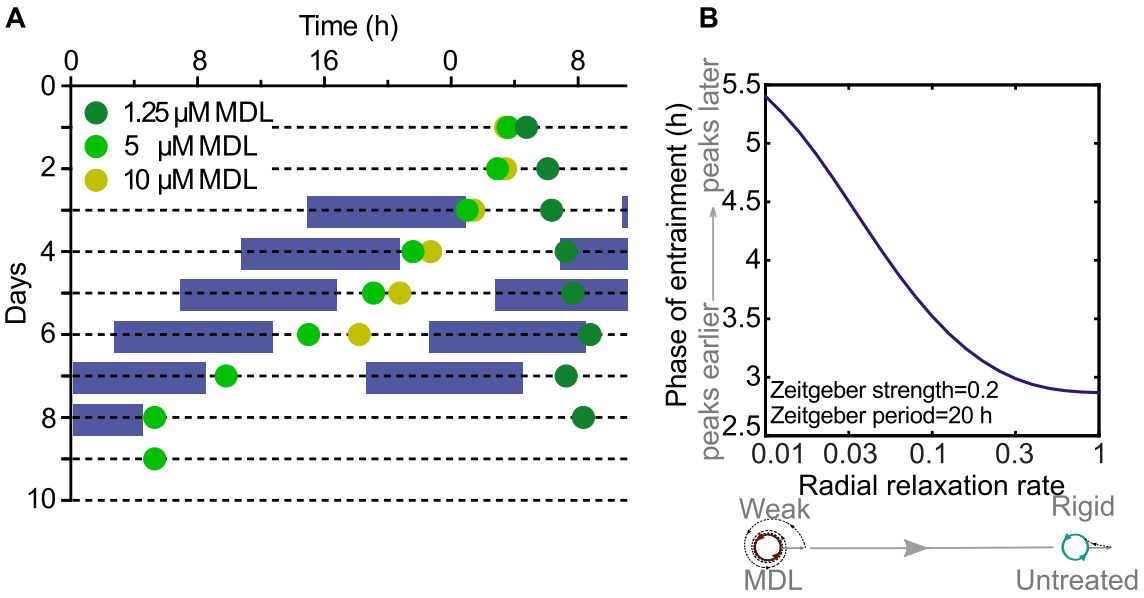


Figure S8: Entrainment phase is dependent on coupling. (**A**) SCN slices cultured in the presence of different MDL concentrations show differential entrainment to $T$ = 20 hour temperature cycles. SCN slices were cultured in medium supplemented with 1.25 $\mu$M (dark green), 5 $\mu$M (light green), and 10 $\mu$M (olive) MDL, respectively, which are speculated to convey different degrees of decoupling (high concentration = strong decoupling; low concentration = weak decoupling). In line with our theory (see panel B), SCN treated with 5 and 10 $\mu$M MDL, i.e. presumably strongly decoupled tissues, are able to entrain their PER2::LUCIFERASE bioluminescence rhythms to a $T$ = 20 hour temperature cycle (also see Figure 6E), while the presumably less decoupled SCN (1.25 $\mu$M) does not. Also note that the SCN treated with 10 $\mu$M MDL peaks later with respect to the onset of the temperature zeitgeber than the SCN treated with 5 $\mu$M MDL. This is consistent with our experimental findings that stronger zeitgebers result in earlier peak phases (see Supplementary Figure S6), and also with the simulation described in panel (B) (see below). Displayed are peak times of PER2::LUCIFERASE bioluminescence derived from three individual SCN slices. Between days 3 and 8, in vitro cultures were subjected to 20-hour temperature cycles with 10-hour cold phases (blue boxes) of 35.5 °C ($\Delta$T = 1.5 K), alternating with 10-hour warm phases of 37 °C. Following day 8, cultures were kept at a constant 37 °C. (**B**) Numerically calculated phase of entrainment for a Poincaré oscillator (see Equation 1 of the paper) as a function of its radial relaxation rate $\lambda$. Weak oscillators have a later phase of entrainment than rigid oscillators. Note that in our interpretation, MDL treated SCN slices behave as weak oscillators whereas untreated SCN slices behave as rigid oscillators. The simulation is thus consistent with the phases of slices treated with 5 $\mu$l and 10 $\mu$l respectively, as described in panel (A) above. For this simulation we study a Poincaré oscillator entrained to a 20 h and 0.2 $h^{-1}$ zeitgeber period and amplitude, respectively. Computational details are given in Supplementary Material and methods.

**Supplementary Movies S1-S4**

Pharmacological decoupling of SCN cells leads to de-phasing of single cell oscillations. Using an ultrasensitive ICCD camera, 10 min exposures of PER2::LUCIFERASE bioluminescence derived from cultured SCN slices were sampled over the course of several days. Two representative SCN slices were individually recorded for about 5 days (untreated; movies S1 and S3) before the medium was changed to culture medium supplemented with 10 $\mu$M MDL (MDL; movies S2 and S4), and recording was resumed. The movies were analyzed as described below and shown in Figure 6A-C.

**Table S1:** Periods of PER2::LUCIFERASE bioluminescence rhythms before, during, and after temperature entrainment. Convergence of bioluminescence periods with the imposed temperature cycle suggests entrainment. Experimental conditions are indicated.

| | | | | Period (h) | | |
|---|---|---|---|---|---|---|
| **Temperature cycle** | **Δ T** | **Tissue** | **Drug treatment** | before entr. | during entr. | after entr. |
| T20 | 1.5 | SCN 1 | - | 23.38 | 24.04 | 24.10 |
| | 1.5 | SCN 2 | - | 23.41 | 24.03 | 23.89 |
| | 1.5 | SCN 3 | - | 24.09 | 23.92 | 24.08 |
| | 1.5 | SCN 4 | - | 23.84 | 22.46 | 22.69 |
| | 1.5 | Lung 1 | - | 22.91 | 21.62 | 22.36 |
| | 1.5 | Lung 2 | - | 23.01 | 19.90 | 22.05 |
| | 1.5 | Lung 3 | - | 22.61 | 22.51 | 22.21 |
| | 1.5 | Lung 4 | - | 22.42 | 22.96 | 21.92 |
| T28 | 1.5 | SCN 1 | - | 23.65 | 24.08 | 24.24 |
| | 1.5 | SCN 2 | - | 23.47 | 23.52 | 23.78 |
| | 1.5 | SCN 3 | - | 23.89 | 24.1 | 23.97 |
| | 1.5 | SCN 4 | - | 23.61 | 23.71 | 23.87 |
| | 1.5 | Lung 1 | - | 24.75 | 26.77 | 24.32 |
| | 1.5 | Lung 2 | - | 24.94 | 26.79 | 24.53 |
| | 1.5 | Lung 3 | - | 24.24 | 27.05 | 24.23 |
| | 1.5 | Lung 4 | - | 24.43 | 27.3 | 23.98 |
| T20 | 0.75 | SCN 1 | - | 24.79 | 24.55 | n/a |
| | 3 | SCN 2 | - | 23.69 | 23.94 | n/a |
| | 6 | SCN 3 | - | 23.95 | 25.54 | n/a |
| | 0.75 | Lung 1 | - | 23.61 | 21.35 | 24.12 |
| | 1.5 | Lung 2 | - | 23.47 | 21.77 | 24.49 |
| | 3 | Lung 3 | - | 22.44 | 21.02 | 24.61 |
| | 6 | Lung 4 | - | 23.07 | 20.72 | 24.2 |
| T22 | 4 | SCN 1 * | - | 26.87 | 22.93 | 24.14 |
| | 6 | SCN 2 | - | 24.15 | 22.46 | 24.02 |
| | 8 | SCN 3 | - | 23.77 | 22.73 | 23.76 |
| T20 | 1.5 | SCN 1 | MDL (10μM) | 24.12 | 20.40 | 24.00 |
| | 1.5 | SCN 2 | MDL (10μM) | 24.46 | 20.73 | 23.99 |
| | 1.5 | SCN 3 | MDL (10μM) | 24.92 | 24.30 | 23.17 |
| | 1.5 | SCN 4 | MDL (10μM) | 25.93 | 19.58 | 24.00 |
| | 1.5 | SCN 5 | MDL (10μM) | 24.73 | 24.71 | 24.33 |
| | 1.5 | SCN 6 | MDL (10μM) | 25.34 | 19.75 | 25.61 |
| | 1.5 | SCN 7 | MDL (10μM) | 23.77 | 19.85 | 24.00 |
| | 1.5 | SCN 8 | MDL (10μM) | 24.65 | 20.96 | 24.00 |
| T20 | 1.5 | SCN 1 | MDL (10μM) | 24.55 | 22.07 | n/a |
| | 1.5 | SCN 2 | MDL (5μM) | 23.41 | 21.51 | n/a |
| | 1.5 | SCN 3 | MDL (1.25μM) | 23.94 | 24.77 | n/a |
| T20 | 1.5 | SCN 1 | TTX (2-4μM) | 22.31 | 20.77 | 24.00 |
| | 1.5 | SCN 2 | TTX (2-4μM) | 23.36 | 18.94 | 24.04 |
| | 1.5 | SCN 3 | TTX (2-4μM) | 24.03 | 22.46 | 23.36 |
| | 1.5 | SCN 4 | TTX (2-4μM) | 22.77 | 21.95 | 22.90 |
| | 1.5 | SCN 5 | TTX (2-4μM) | 23.54 | 20.28 | 24.70 |
| | 1.5 | SCN 6 | TTX (2-4μM) | 22.88 | 21.24 | 24.00 |

* SCN tissue showed “masking” in response to the temperature cycle. Hence, periods reflect entrainment , while the tissue did not seem to be entrained in the phase analysis (see Fig. S6).